Supporting Information

Zero power infrared sensing in 2D/3D-assembled heterogeneous graphene/In/InSe/Au

Hanbyeol Jang[a], *Yumin Song*[b], *Yongwook Seok*[a], *Heungsoon Im*[a], *Tae Hyung Kim*[b], *Joo-Hyoung Lee*[a], *Yong-Hoon Kim*[b], *Kayoung Lee*[b,*]

[a]School of Materials Science and Engineering, Gwangju Institute of Science and Technology (GIST), Gwangju 61005, Republic of Korea

[b]School of Electrical Engineering, Korea Advanced Institute of Science and Technology (KAIST), Daejeon 34141, Republic of Korea

[*]Corresponding author (email: kayoung.lee@kaist.ac.kr)

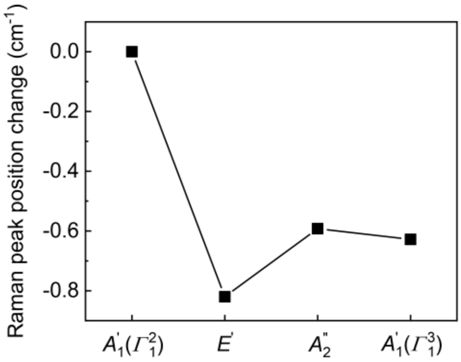

Fig. S1 Relative Raman peak position changes after In deposition on InSe.

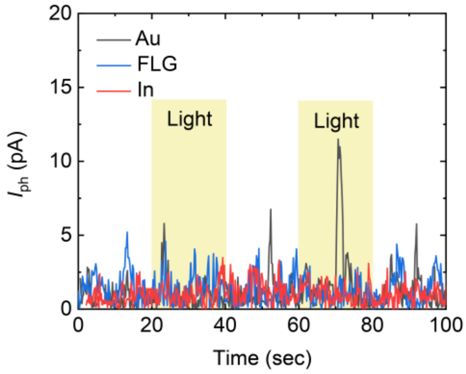

Fig. S2 Photo-switching characteristics of the InSe field-effect devices with different metal contacts, Au, FLG, and In (λ = 850 nm, P = 0.5 mW cm^{-2}, V_{DS} = 0 V).

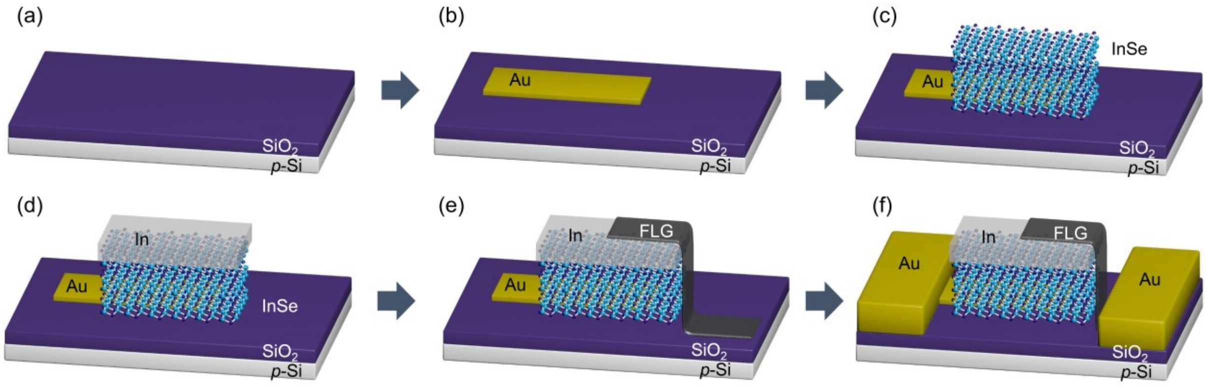

Fig. S3 Schematic of the fabrication process for our self-powered InSe photodetector. (a) A SiO_2/*p*-Si substrate, (b) deposition of an Au bottom electrode on the SiO_2/*p*-Si substrate, (c) transfer of an InSe flake on the Au bottom electrode, (d) 15-nm-thick In deposition, (e) stacking a FLG flake on the In/InSe, and (f) metal electrode deposition on the Au bottom electrode and the FLG flake.

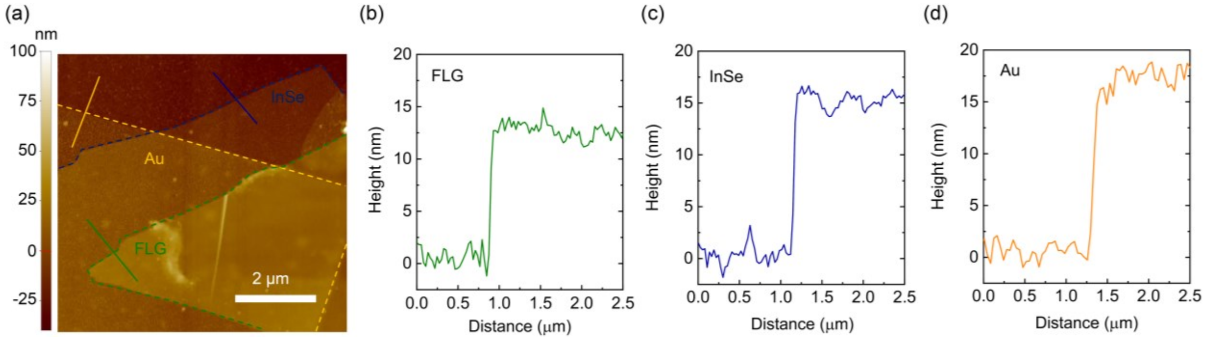

Fig. S4 (a) Atomic force microscope (AFM) image of the FLG/In/InSe/Au heterostructure and (b-d) surface profiles of the InSe, FLG, and Au in the heterostructure along the blue, green, and orange lines in the AFM image.

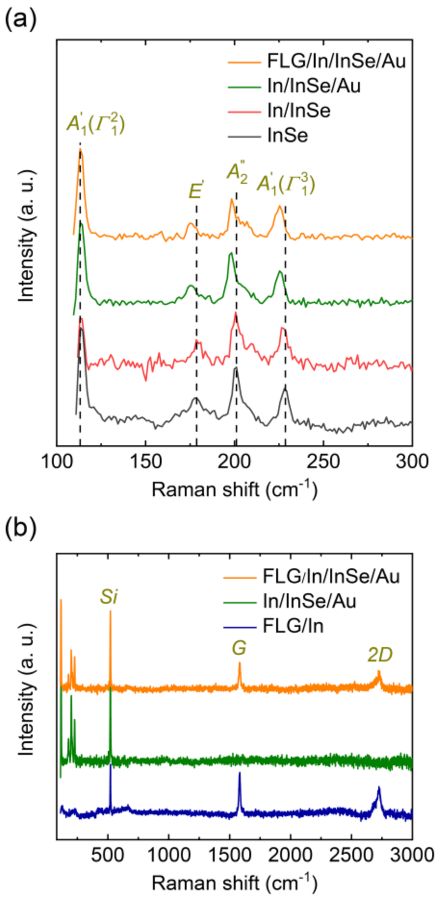

Fig. S5 (a) Raman spectra of the FLG/In/InSe/Au, In/InSe/Au, In/InSe, and InSe. (b) Raman spectra of the FLG/In/InSe/Au, In/InSe/Au, and FLG/In regions of the photodetector.

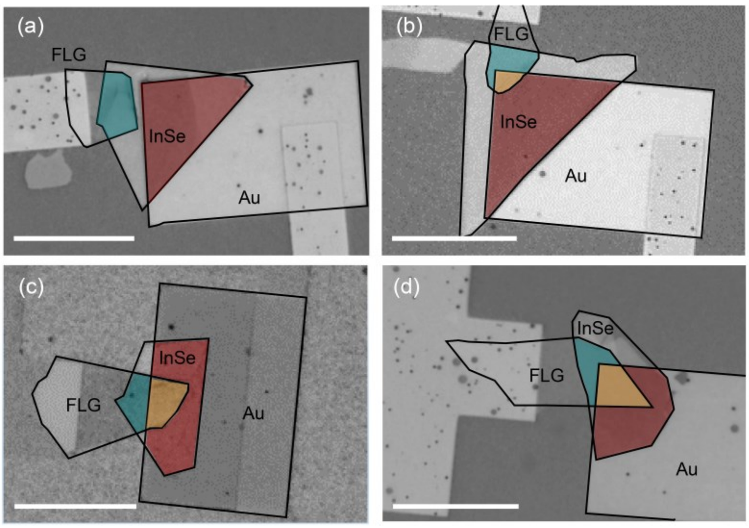

Fig. S6 Optical micrographs of the multiple self-powered InSe photodetectors: (a) sample #1, (b) sample #2, (c) sample #3, and (d) sample #4. Region 1 (yellow), Region 2 (blue), and Region 3 (red) are marked in each optical micrograph. The scale bar denotes 10 μm.

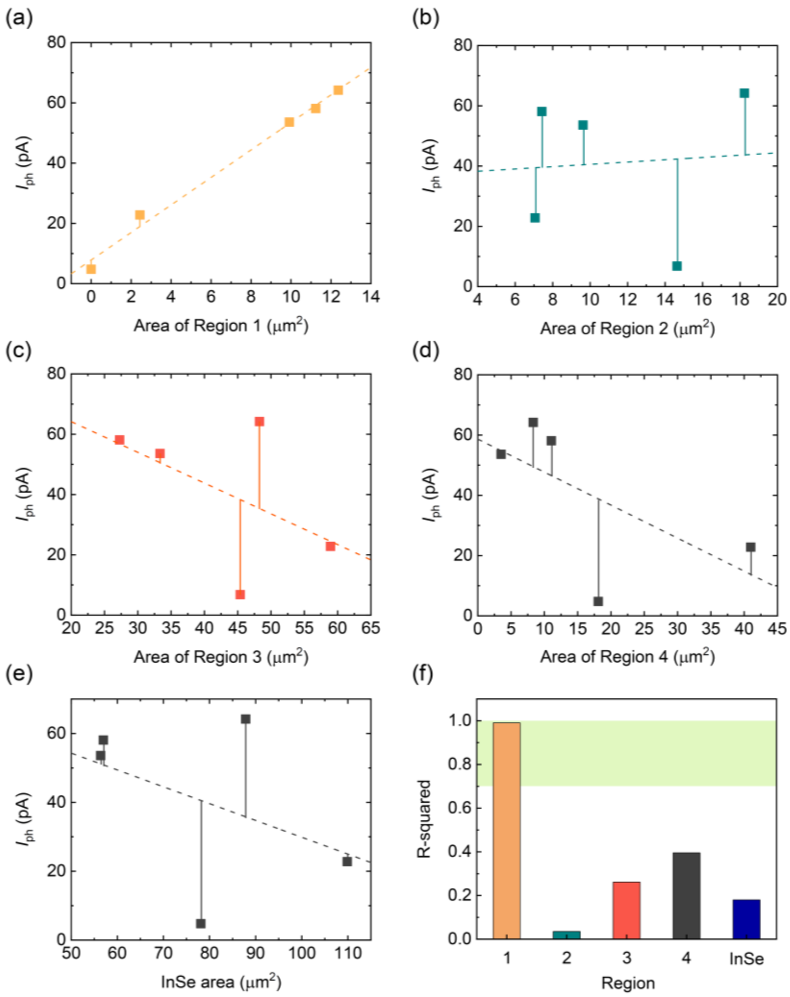

Fig. S7 I_{ph} as a function of the areas of (a) Region 1, (b) Region 2, (c) Region 3, (d) Region 4, and (e) InSe. (f) R-squared of the regression line in graphs (a–e).

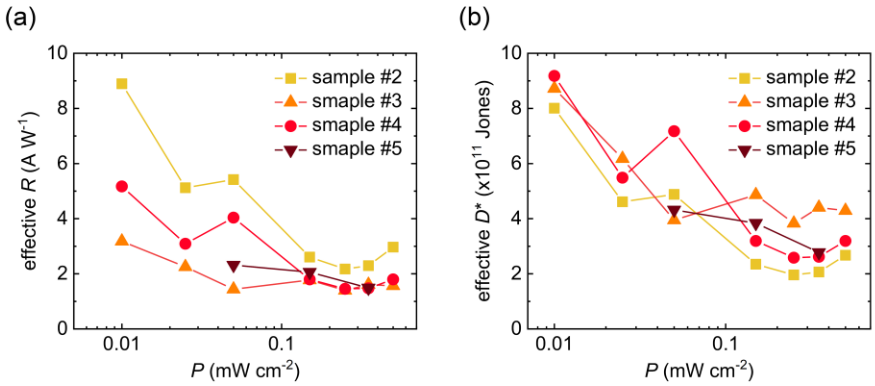

Fig. S8 Effective (a) *R* and (b) *D** of the multiple self-powered photodetectors as a function of *P*.

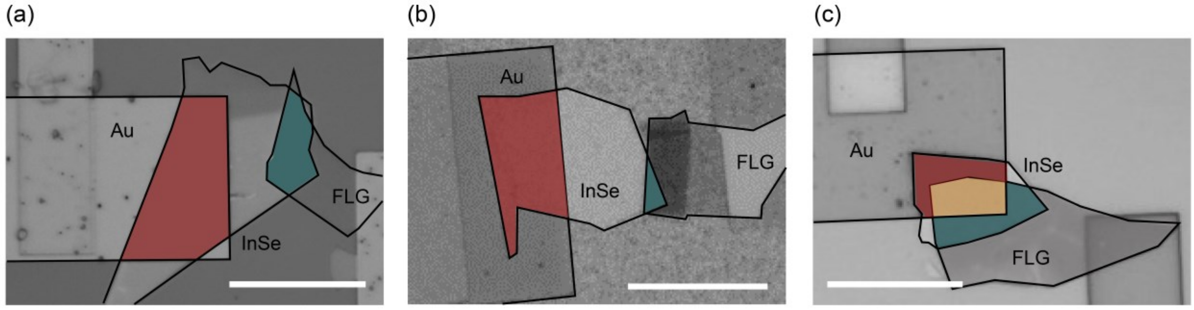

Fig. S9 Optical micrographs of the (a) type 1, (b) type 2, and (c) type 3 devices. The InSe/Au (red), In/InSe/Au (red), FLG/InSe/Au (yellow), FLG/InSe (blue), and FLG/In/InSe (blue) regions are marked in each optical micrograph. The scale bar denotes 10 μm.

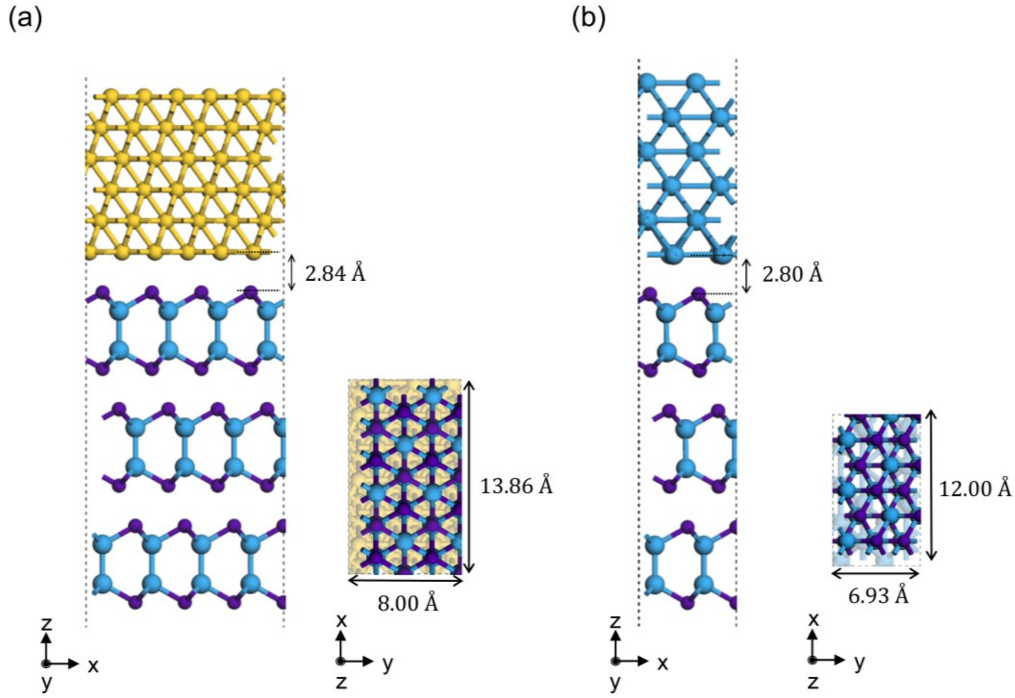

Fig. S10 (a) InSe-Au and (b) InSe-In models for density functional theory (DFT) calculations. For geometry optimization, the uppermost four layers of Au and In were fixed in bulk geometry, and the two other layers of the metallic surface were allowed to relax.

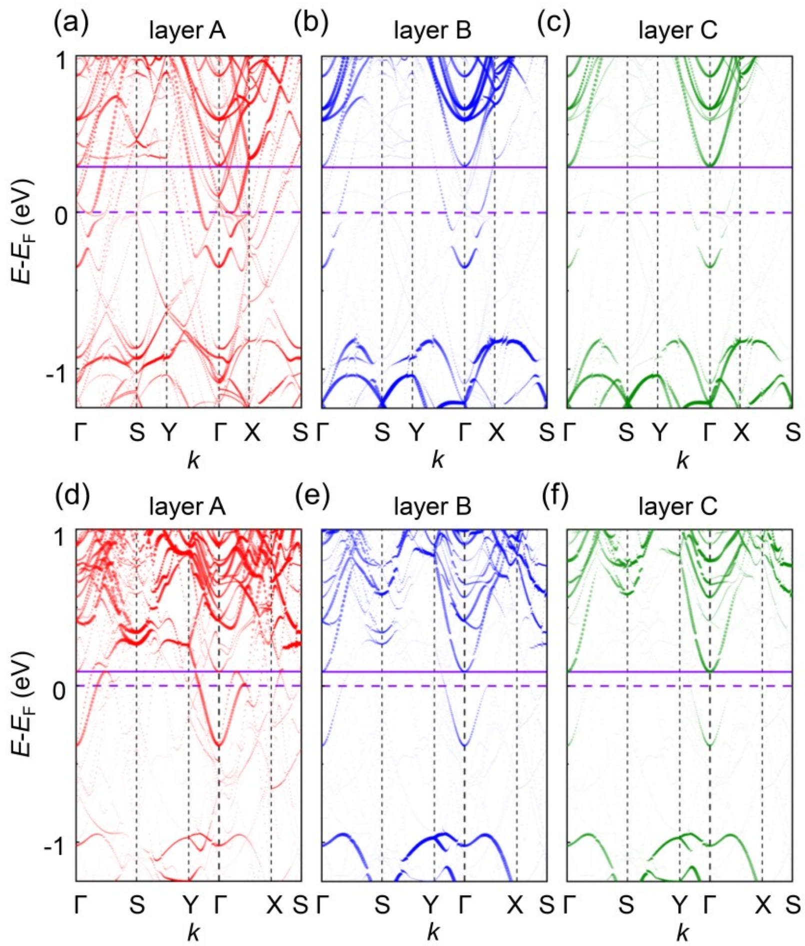

Fig. S11 Calculated projected band structures of InSe (a) layer A, (b) layer B, and (c) layer C extracted from the InSe-Au model, and those of InSe (d) layer A, (e) layer B, and (f) layer C extracted from the InSe-In model. All bands are aligned with respect to the Fermi level E_F of the contact (Au or In) (dashed purple lines) and the solid purple lines indicate the conduction band minimum edge determined based on the layer C projected bands.

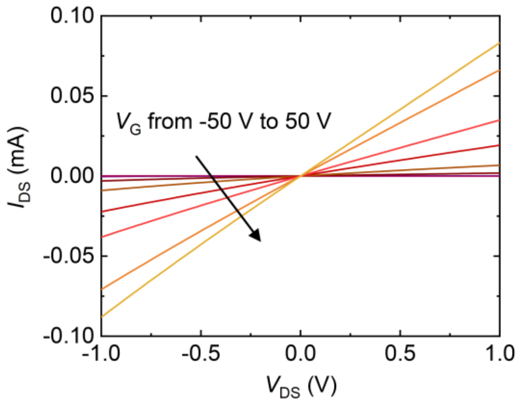

Fig. S12 I_{DS} versus V_{DS} curves of the In-contacted InSe device at V_G from -50 V to 50 V in steps of 10 V.

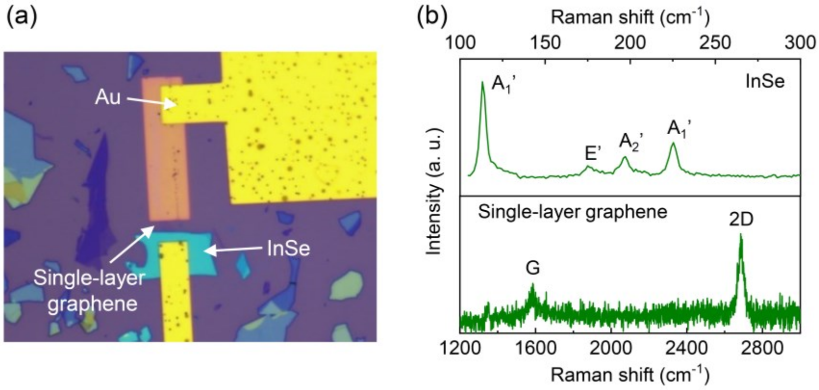

Fig. S13 (a) Optical micrograph of the InSe VFET. (b) Raman spectra of the InSe and SLG in the InSe VFET.

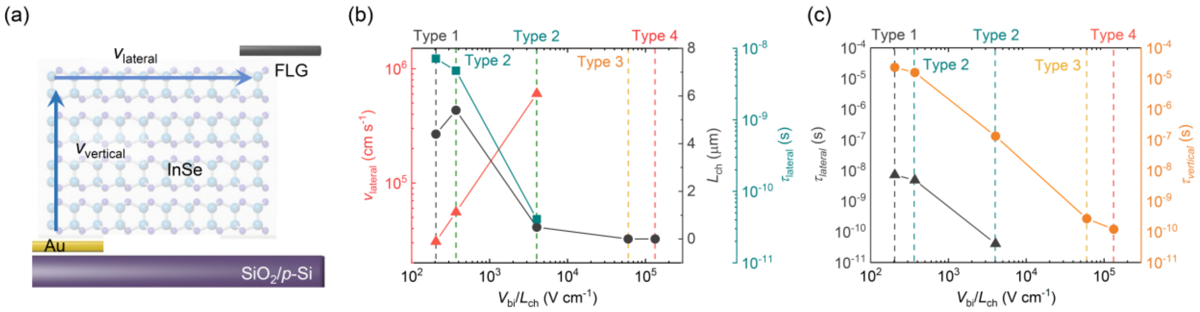

Fig. S14 (a) Schematic side view of the type 1 device. The arrows schematically describe the directions of v_{vertical} and v_{lateral}, the components of drift velocity along the out-of-plane and in-plane directions, respectively. (b) v_{lateral}, L_{ch} and τ_{lateral} of the type 1 and 2 photodetectors as functions of $V_{\mathrm{bi}}/L_{\mathrm{ch}}$, where $v_{\mathrm{lateral}} = \mu_{\mathrm{lateral}} V_{\mathrm{bi}}/L_{\mathrm{ch}}$ is the lateral drift velocity, $\mu_{\mathrm{lateral}} = 150$ cm^2/Vs is the in-plane mobility, and $\tau_{\mathrm{lateral}} = L_{\mathrm{ch}}/2v_{\mathrm{lateral}}$ is the transit time along the lateral direction. (c) τ_{lateral} and τ_{vertical} of the type 1, 2, 3, and 4 photodetectors as functions of $V_{\mathrm{bi}}/L_{\mathrm{ch}}$.

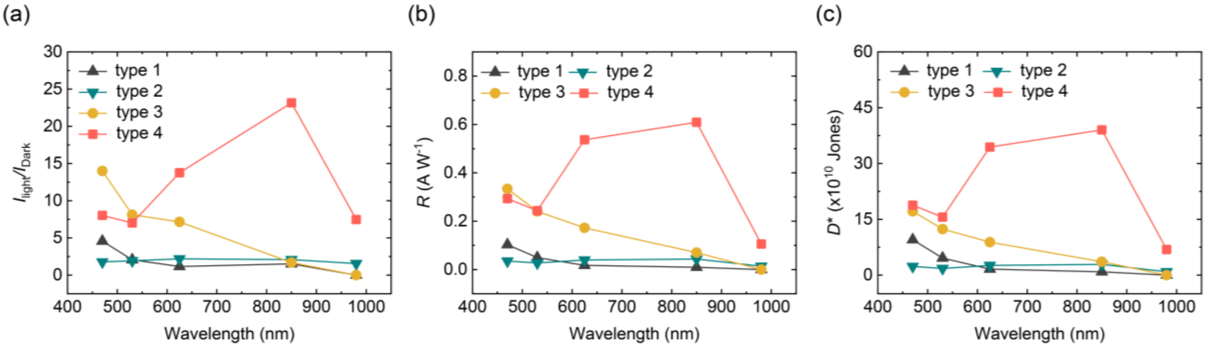

Fig. S15 (a) $I_{\mathrm{light}}/I_{\mathrm{dark}}$ (P = 0.5 mW cm^{-2}), (b) R, and (c) D^* (P = 0.025 mW cm^{-2}) of the type 1–4 photodetectors as functions of wavelength.

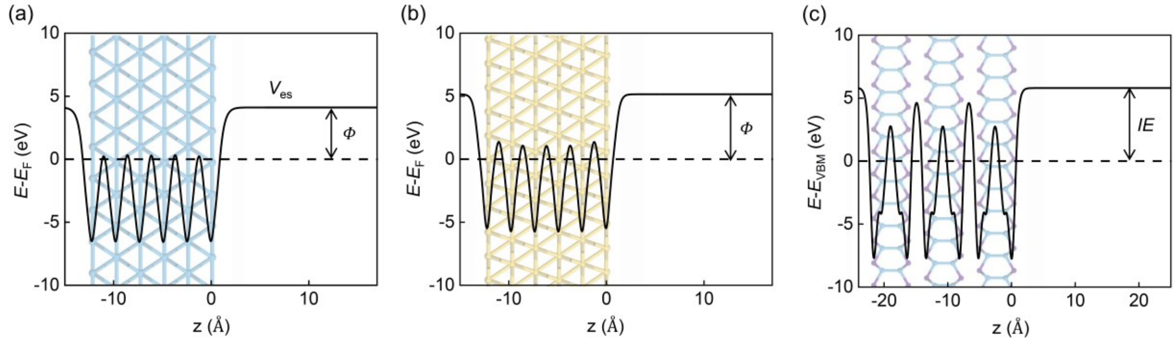

Fig. S16 DFT-derived plane-averaged electrostatic potentials (V_{es}) of the a) In six-layer slab model, b) Au six-layer slab model, and c) InSe three-layer slab model. Work functions (Φ) are extracted by $E_{vac} - E_F$ (horizontal dashed lines in (a) and (b)). The calculated Φ_{In} = 4.10 eV and Φ_{Au} = 5.15 eV match well with experimentally reported values.[1,2] Ionization energy (IE) is extracted by $E_{vac} - E_{VBM}$ (horizontal dashed line in (c)). The calculated IE_{InSe} = 5.80 eV is well match with a experimentally reported value.[3]

References

(1) Michaelson, H. B. The Work Function of the Elements and Its Periodicity. *Journal of Applied Physics* **1977**, *48*, 4729–4733.

(2) Li, C.; Pan, F.; Wang, X.; Wang, L.; Wang, H.; Wang, H.; Yan, D. Effect of the Work Function of Gate Electrode on Hysteresis Characteristics of Organic Thin-Film Transistors with Ta2O5/Polymer as Gate Insulator. *Organic Electronics* **2009**, *10*, 948–953.

(3) Lang, O.; Pettenkofer, C.; Sánchez-Royo, J. F.; Segura, A.; Klein, A.; Jaegermann, W. Thin Film Growth and Band Lineup of In2O3 on the Layered Semiconductor InSe. *Journal of Applied Physics* **1999**, *86*, 5687–5691.